Comparison of continuous and stop-and-go scanning techniques in photoacoustic tomography

Sharma, Arunima; Kalva, Sandeep Kumar; Pramanik, Manojit

2018

Sharma, A., Kalva, S. K., & Pramanik, M. (2018). Comparison of continuous and stop-and-go scanning techniques in photoacoustic tomography. Proceedings of SPIE - Photons Plus Ultrasound: Imaging and Sensing 2018, 10494, 104943L-.

https://hdl.handle.net/10356/87723

https://doi.org/10.1117/12.2288095

Comparison of continuous and stop-and-go scanning techniques in photoacoustic tomography

Arunima Sharma, Sandeep Kumar Kalva, and Manojit Pramanik*
School of Chemical and Biomedical Engineering, Nanyang Technological University, 62 Nanyang Drive, Singapore 637459

ABSTRACT

Photoacoustic tomography is an emerging imaging modality which has paved its way in preclinical and clinical trials owing to the multiple advantages it offers. A typical PAT system consists of a laser beam which homogeneously illuminates the sample giving rise to photoacoustic (PA) waves, which are collected using an ultrasound transducer (UST) rotating around the sample. Low cost, high sensitivity and easy availability have made single-element transducers (SETs) a preferred choice for acquiring these A-lines PA signal. Two methods have been reported for collection of these A-lines by SETs- (1) Stop-and-go scan and (2) Continuous scan. In stop-and-go scan, the stepper motor moves the SET to a predefined position where the SET collects multiple A-lines. Once the desired number of A-lines at that point have been collected and saved, the stepper motor moves to the next position and the process continues. A continuous scan is one in which the stepper motor rotates the SET continuously at a predefined speed. The A-lines are thus collected by a moving SET and are saved once the motor has stopped. In this work, we have compared the two types of scanning methods in terms of image quality, signal-to-noise ratio and time of scan by performing experiments on phantoms.

Keywords: Continuous scanning, stop-and-go scanning, single-element ultrasound transducer, circular scanning geometry, photoacoustic tomography, thermoacoustic tomography

1. INTRODUCTION

Photoacoustic tomography (PAT) is a noninvasive three-dimensional hybrid imaging modality which combines the advantages of optical and acoustic imaging [1-5]. In PAT, a non-ionising pulsed laser irradiates a biological tissue. Chromophores present is the tissue absorb the radiations resulting in a slight temperature rise, thereby generating thermoelastic expansion pressure waves, also known as photoacoustic (PA) waves [6-8]. PA waves around the sample are detected using an ultrasound transducer (UST) and later reconstructed to give a cross sectional view of the same. Having the merits of good optical contrast, high ultrasound resolution, and deep penetration depth, photoacoustic imaging has a wide range of preclinical and clinical applications like brain imaging [9-11], breast imaging [12], sentinel lymph node imaging [13, 14], molecular imaging [15], cell imaging [16] etc.

PAT generally employs circular scanning geometry in orthogonal mode to acquire the PA signal around the sample [17]. For signal acquisition, different types of transducers can be used in a PAT system. These include single element transducers (SETs) [18], linear array transducers [19-21], semi-circular array transducers [22], circular array transducers [23] etc. Although the array transducer based PAT systems are faster, SETs are still used being cost-effective, easily available, and highly sensitive. However, decreasing the data acquisition time (scan time) for SET based PAT systems remains a concern. Different methods are being used to decrease the scan time of SET based PAT systems. One of these is to use lasers of high pulse repetition rate (PRR). Light emitting diodes (LED) [24] and pulsed laser diodes (PLD) [25, 26] offer higher PRR as compared to the traditional Nd:YAG lasers, thereby considerably reducing scan time of PAT system. Further, using continuous scans has also proven to be efficient in decreasing scan-time.

There are two ways of signal acquisition in SET-based PAT systems- 1) stop-and-go scans [27] and 2) continuous scans [28, 29]. In stop-and-go scans, the UST moves around the sample in steps of predefined length. After each step, the UST collects and averages a given number of PA signals and then proceeds to move another step, till it has completed one full rotation around the sample. In continuous scans, the UST moves around the sample continuously at a predefined speed

* manojit@ntu.edu.sg;

Photons Plus Ultrasound: Imaging and Sensing 2018, edited by Alexander A. Oraevsky, Lihong V. Wang, Proc. of SPIE Vol. 10494, 104943L · © 2018 SPIE · CCC code: 0277-786X/18/$18 · doi: 10.1117/12.2288095

and collects PA signal while moving. The UST stops only after it has collected all the PA signals all around the sample. Following signal acquisition, similar reconstruction algorithm can be used for both the types of scans to get the image. In this paper, we have compared the stop-and-go and continuous scanning method for SET-based PAT system. Two phantoms were prepared to acquire images which were used to compare the above-mentioned parameters of the scanning methods.

2. MATERIALS AND METHODS

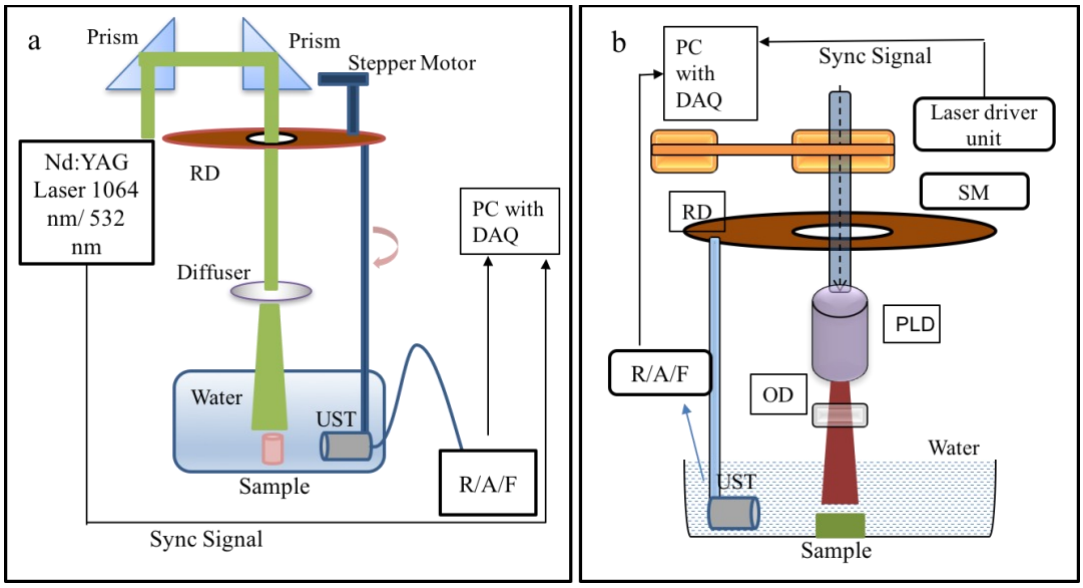

Figure 1: Schematic of (a) Nd:YAG based PAT system and (b) PLD based PAT system. RD: rotating disc, SM: stepper motor, PLD: pulsed laser diode, UST: ultrasound transducer, OD: optical diffuser, R/A/F: receiver, amplifier, filter.

2.1 PAT system setup

Fig. 1(a) shows the experimental setup in which a Q-switched Nd:YAG laser (Continuum, Surelite Ex) delivered 5 ns pulses with 10 Hz pulse repetition rate (PRR) at a wavelength of 532 nm or 1064 nm. The pulse fluence was maintained at ~6 mJ/cm^2 and ~25 mJ/cm^2, respectively. Fig 1(b) shows the setup wherein a PLD (Quantel, France) was used to irradiate the sample at a wavelength of 803 nm and 7 kHz PRR. Here, the pulse fluence was ~0.08 mJ/cm^2. Laser fluence was maintained such that it was within the ANSI safety limit [30]. The laser beam was made to homogeneously illuminate the sample using optical components like diffusers and prisms.

An ultrasound transducer rotating around the sample was used to collect the time resolved PA signals, known as A-lines. A stepper motor connected to the UST moved it around the sample continuously at a constant speed (for continuous scans) and in steps of 1°, 2°, or 4°, for stop-and-go scans. Therefore, one rotation of the UST for stop-and-go scan was completed in 360 steps, 180 steps, and 90 steps, respectively. For comparison of image quality, same number of A-lines were collected for both the types of scans. The PA signal was amplified by ~45dB and then recorded using a date acquisition (DAQ) card at a sampling rate of 25 MS/s. The motion of motor, trigger signal from the laser and the PA signal from the sample were all synchronized by the DAQ card. Once the A-lines were collected, delay-and-sum algorithm [28, 31, 32] was employed to reconstruct the cross-sectional PAT images.

2.2 Sample preparation

Images of phantoms were taken and compared for image quality, signal to noise ratio, scan time, and laser exposure. Five pencil leads of approximately 0.5 mm diameter were stuck vertically on an acrylic slab using pipette tubes for support. The leads were placed such that one lead was at the center and other four were placed symmetrically at a distance of about 1 cm from the center one. The Nd:YAG based PAT system working at the wavelength of 532 nm was used for point source phantom imaging. The second phantom was prepared by sticking three horse hair in the shape of a triangle on top of transparent pipette tubes. The hair had a diameter of about 150 micrometers and a length of 1 cm. For this imaging, PLD based PAT system at a wavelength of 803 nm was used.

All the samples were placed such that they were homogeneously illuminated by the laser and were aligned in a straight line with the UST used to detect the PA signal. To provide coupling of the PA signal, the UST and the phantoms were kept in a water tank. The samples were fixed at a point such that they did not move due to vibrations in water due to movement of the motor.

3. RESULTS AND DISCUSSIONS

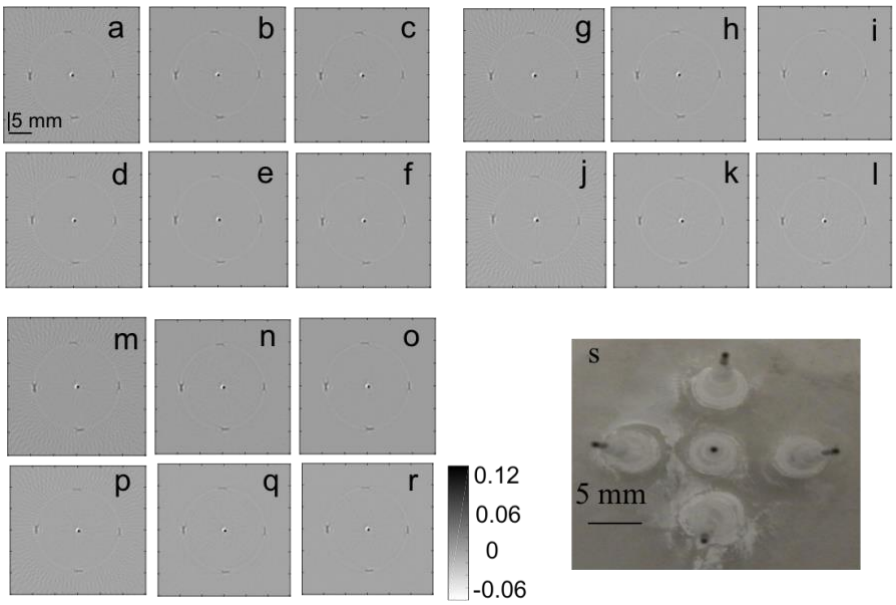

Figure 2: Reconstructed images of point source phantom. 360(a-f), 720(g-l), and 1440(m-r) A-lines were collected using stop-and go (a-c, g-i, m-o), and continuous (d-f, j-l, p-r) scanning methods. 90 (a, d, g, j, m, p), 180 (b, e, h, k, n, q), and 360 (c, f, i, l, o, r) were reconstructed. Photograph of phantom is shown in s.

Figure 2 shows the images of point source phantom acquired using stop-and-go scan [Figs. 2(a-c, g-i, m-o)], and continuous scan [Figs. 2(d-f, j-l, p-r)]. 360, 720, and 1440 A-lines were collected in Figs. 2(a-f), Figs. 2(g-l), and Figs. 2(m-r), respectively. For stop-and-go scans, all the A-lines taken at one step were averaged together before reconstruction of the images. For fair comparison, similar averaging (as for stop-and-go) was also done for continuous scans. Thus, Fig. 2 shows reconstruction of 90 [Figs. 2(a, d, g, j, m, p)], 180 [Figs. 2(b, e, h, k, n, q)], and 360 [Figs. 2(c, f, I, l, o, r)] A-lines, respectively. Photograph of the phantom is shown in Fig. 2(s).

For triangle phantom, images were acquired using the PLD-PAT system at the PRR of 7000 Hz. 63000 and 126000 A-lines were collected by moving the motor continuously for 9 and 18 seconds, respectively for continuous scans. Same number of A-lines were collected for stop-and-go scans as well. Figs. 3(a-f) shows the images where 63000 A-lines were collected and Figs. 3(g-l) shows images where 126000 A-lines were collected. Finally, 90 [Figs. 3(a, d, g, j)], 180 [Figs. 3(b, e, h, k)], and 360 [Figs. 3(c, f, i, l)] A-lines were reconstructed for both the types of scans. Figs. 3(a-c) and Figs. 3(g-i) show the images obtained by stop-and-go scans and Figs. 3(d-f) and Figs. 3(j-l) show the corresponding images of continuous scans. Photograph of the phantom is shown in Fig. 3(m).

From the images, it can be observed that the image quality improves on increasing the number of A-lines collected. This difference in images was found to be more prominent while using Nd:YAG based PAT system as compared to PLD-based PAT system. When the number of A-lines collected was kept constant, there was still an observable improvement in images when the number of A-lines reconstructed was increased. This was true for both the ND:YAG based PAT system as well as the PLD based PAT system.
It may however be noted that no remarkable difference in image quality could be observed between the two types of scans when the number of A-lines collected was kept constant. The signal to noise ratio (values not shown) was also calculated and it validated that there was negligible difference between the images acquired using the two types of scans.

Table 1 shows the scan time and the laser pulse exposure of the two types of scans. A significant improvement in scan time can be observed on moving from stop-and-go to continuous scan. This improvement was 7-12 folds on using PLD-based PAT system and 3-4 folds on using traditional Nd:YAG based PAT system. The decrease in scan time further results in a decrease in laser exposure. Having a high PRR, even a slight decrease in scan time of PLD based PAT system results in a tremendous decrease in laser exposure.

Since the A-lines in continuous scans are acquired by a moving transducer, the decrease in scan time was expected. This motion, however, could also result in blurring, thus degrading the image quality. No major change in image quality between the two types of scans may be attributed to the fact that the relative movement of UST is much less than present resolution of PAT system [33]. Therefore, even though the A-lines are collected by a moving transducer the effects due to motion can be ignored.

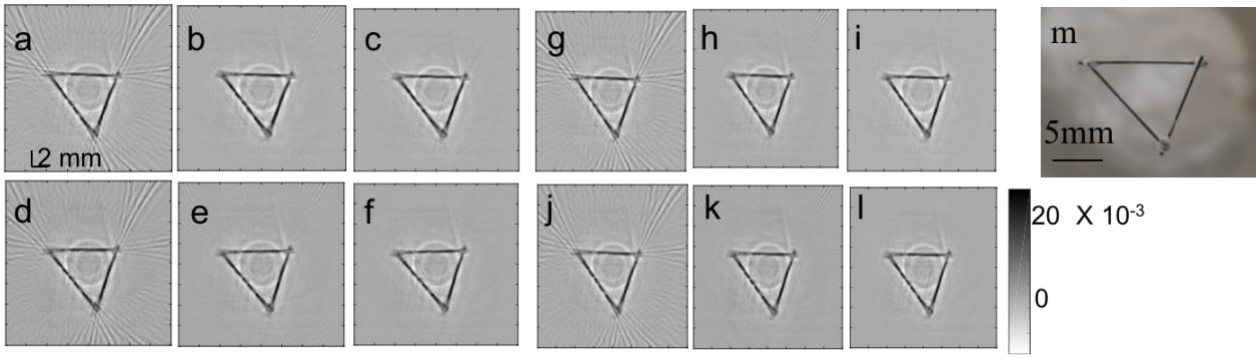

Figure 3: Images of triangle phantom formed by collecting (a-f) 63000, and (g-l) 126000 A-lines. Stop-and-go (a-c, g-i), and continuous (d-f, j-l) scanning methods were used for collection and finally (a, d, g, j) 90, (b, e, h, k) 180, and (c, f, i, l) 360 A-lines were reconstructed. Photograph of phantom is shown in m.

Table 1: Scan time and the number of pulses sample got exposed to during stop-and-go scans of 90, 180, and 360 steps and during continuous scan

Laser (PRR)	Nd:YAG (10 Hz)						PLD (7000 Hz)			
A-lines collected	360 A-lines		720 A-lines		1440 A-lines		63000 A-lines		126000 A-lines	
	Time	Pulses	Time	Pulses	Time	Pulses	Time	Pulses	Time	Pulses
Stop-and-go (90 steps)	98 s	980	135 s	1350	210 s	2100	78 s	546000	87 s	609000
Stop-and-go (180 steps)	108 s	1080	147 s	1470	217 s	2170	90 s	630000	99 s	693000
Stop-and-go (360 steps)	109 s	1090	145 s	1450	217 s	2170	125 s	875000	132 s	924000
Continuous scan	36 s	360	72 s	720	144 s	1440	9 s	63000	18 s	126000

4. CONCLUSION

In this work, we have compared the two common scanning methods for single element transducer based PAT system. PA images of both the types of scans were acquired using traditional Nd:YAG based PAT system as well as high pulse repetition rate PLD-based PAT system. Images of point source and shape phantoms were acquired for the comparison. We have shown that for both the systems, performing continuous scans can result in significant decrease of scan time, and therefore laser exposure, without compromising on image quality.

ACKNOWLEDGEMENT

The authors would like to thank Singapore Ministry of Health's National Medical Research Council (NMRC/OFIRG/0005/2016: M4062012) for funding this research. Authors have no relevant financial interests in the manuscript and no other potential conflicts of interest to disclose.

REFERENCES

[1] L. Li, L. Zhu, C. Ma *et al.*, "Single-impulse panoramic photoacoustic computed tomography of small-animal whole-body dynamics at high spatiotemporal resolution," Nature Biomedical Engineering, 1, 0071 (2017).
[2] P. K. Upputuri, and M. Pramanik, "Recent advances toward preclinical and clinical translation of photoacoustic tomography: a review," Journal of Biomedical Optics, 22(4), 041006 (2017).
[3] S. Hu, "Listening to the Brain With Photoacoustics," IEEE Journal of Selected Topics in Quantum Electronics, 22(3), 6800610 (2016).
[4] L. V. Wang, and J. Yao, "A practical guide to photoacoustic tomography in the life sciences," Nature Methods, 13(8), 627-38 (2016).
[5] L. V. Wang, and L. Gao, "Photoacoustic microscopy and computed tomography: from bench to bedside," Annu Rev Biomed Eng, 16, 155-85 (2014).
[6] J. Xia, and L. V.Wang, "Small-Animal Whole-Body Photoacoustic Tomography: A Review," IEEE Transactions on Biomedical Engineering, 61(5), 1380-89 (2014).
[7] L. V. Wang, and S. Hu, "Photoacoustic Tomography: In Vivo Imaging from Organelles to Organs," Science, 335(6075), 1458-1462 (2012).
[8] M. Pramanik, and L. V. Wang, "Thermoacoustic and photoacoustic sensing of temperature," Journal of Biomedical Optics, 14(5), 054024 (2009).
[9] P. K. Upputuri, and M. Pramanik, "Dynamic in vivo imaging of small animal brain using pulsed laser diode-based photoacoustic tomography system," Journal of Biomedical Optics, 22(9), 090501 (2017).
[10] M. Anastasio, K. Mitsuhashi, C. Huang *et al.*, "Recent advancement in transcranial brain imaging using photoacoustic computed tomography," The Journal of the Acoustical Society of America, 135(4), 2208-2208 (2014).
[11] J. J. Yao, J. Xia, K. I. Maslov *et al.*, "Noninvasive photoacoustic computed tomography of mouse brain metabolism in vivo," Neuroimage, 64(1), 257-266 (2013).
[12] X. L. Dean-Ben, T. F. Fehm, M. Gostic *et al.*, "Volumetric hand-held optoacoustic angiography as a tool for real-time screening of dense breast," Journal of Biophotonics, 9(3), 253-9 (2016).
[13] K. Sivasubramanian, V. Periyasamy, and M. Pramanik, "Non-invasive sentinel lymph node mapping and needle guidance using clinical handheld photoacoustic imaging system in small animal," Journal of Biophotonics, (2018 (In Press)).
[14] A. Garcia-Uribe, T. N. Erpelding, A. Krumholz *et al.*, "Dual-Modality Photoacoustic and Ultrasound Imaging System for Noninvasive Sentinel Lymph Node Detection in Patients with Breast Cancer," Scientific Reports, 5, 15748 (2015).
[15] J. Yao, J. Xia, and L. V. Wang, "Multiscale Functional and Molecular Photoacoustic Tomography," Ultrason Imaging, 38(1), 44-62 (2016).
[16] E. M. Strohm, M. J. Moore, and M. C. Kolios, "Single Cell Photoacoustic Microscopy: A Review," IEEE Journal of Selected Topics in Quantum Electronics, 22(3), 6801215 (2016).
[17] C. Li, and L. V. Wang, "Photoacoustic tomography and sensing in biomedicine," Physics in Medicine and Biology, 54(19), R59-97 (2009).

[18] S. K. Kalva, and M. Pramanik, "Use of acoustic reflector to make compact photoacoustic tomography system," Journal of Biomedical Optics, 22(2), 026009 (2017).
[19] K. Sivasubramanian, V. Periyasamy, K. K. Wen *et al.*, "Optimizing light delivery through fiber bundle in photoacoustic imaging with clinical ultrasound system: Monte Carlo simulation and experimental validation," Journal of Biomedical Optics, 22(4), 041008 (2017).
[20] K. Sivasubramanian, and M. Pramanik, "High frame rate photoacoustic imaging at 7000 frames per second using clinical ultrasound system," Biomedical Optics Express, 7(2), 312-323 (2016).
[21] W. Shu, M. Ai, T. Salcudean *et al.*, "Broadening the detection view of 2D photoacoustic tomography using two linear array transducers," Optics Express, 24(12), 12755-68 (2016).
[22] A. Buehler, X. L. Deán-Ben, J. Claussen *et al.*, "Three-dimensional optoacoustic tomography at video rate," Optics Express, 20(20), 22712-19 (2012).
[23] C. Li, A. Aguirre, J. Gamelin *et al.*, "Real-time photoacoustic tomography of cortical hemodynamics in small animals," Journal of Biomedical Optics, 15(1), 010509 (2010).
[24] X. Dai, H. Yang, and H. Jiang, "In vivo photoacoustic imaging of vasculature with a low-cost miniature light emitting diode excitation," Optics Letters, 42(7), 1456-1459 (2017).
[25] P. K. Upputuri, V. Periyasamy, S. K. Kalva *et al.*, "A High-performance compact photoacoustic tomography system for in vivo small-animal brain imaging," Journal of Visualized Experiments(124), e55811 (2017).
[26] P. K. Upputuri, and M. Pramanik, "Pulsed laser diode based optoacoustic imaging of biological tissues," Biomedical Physics & Engineering Express, 1(4), 045010-7 (2015).
[27] G. Ku, X. Wang, G. Stoica *et al.*, "Multiple-bandwidth photoacoustic tomography," Physics in Medicine and Biology, 49(7), 1329-38 (2004).
[28] S. K. Kalva, and M. Pramanik, "Experimental validation of tangential resolution improvement in photoacoustic tomography using a modified delay-and-sum reconstruction algorithm," Journal of Biomedical Optics, 21(8), 086011 (2016).
[29] R. Ma, A. Taruttis, V. Ntziachristos *et al.*, "Multispectral optoacoustic tomography (MSOT) scanner for whole-body small animal imaging," Optics Express, 17(24), 21414-26 (2009).
[30] "American National Standard for Safe Use of Lasers," ANSI Standard Z136.1-2007, NY, (2007).
[31] M. Pramanik, "Improving tangential resolution with a modified delay-and-sum reconstruction algorithm in photoacoustic and thermoacoustic tomography," Journal of the Optical Society of America A, 31(3), 621-7 (2014).
[32] M. A. A. Caballero, A. Rosenthal, J. Gateau *et al.*, "Model-based optoacoustic imaging using focused detector scanning," Optics Letters, 37(19), 4080-2 (2012).
[33] P. K. Upputuri, and M. Pramanik, "Performance characterization of low-cost, high-speed, portable pulsed laser diode photoacoustic tomography (PLD-PAT) system," Biomedical Optics Express, 6(10), 4118-29 (2015).